Journal of Applied Physics

RESEARCH ARTICLE | SEPTEMBER 09 2024

Enhancing superconductivity in $CoSi_2$ films with laser annealing

P. Dumas ✉ ; F. Gustavo ; M. Opprecht; G. Freychet ; P. Gergaud ; S. Kerdilès ; S. Guillemin ; J. L. Lábár ; B. Pécz ; F. Lefloch ; F. Nemouchi

Check for updates

J. Appl. Phys. 136, 105103 (2024)
https://doi.org/10.1063/5.0218950

View Online
Export Citation

10 September 2024 06:11:38

Nanotechnology & Materials Science
Optics & Photonics
Impedance Analysis
Scanning Probe Microscopy
Sensors
Failure Analysis & Semiconductors

Unlock the Full Spectrum.
From DC to 8.5 GHz.
Your Application. Measured.
Find out more
Zurich Instruments

AIP Publishing

Journal of Applied Physics ARTICLE pubs.aip.org/aip/jap

Enhancing superconductivity in $CoSi_2$ films with laser annealing

Cite as: J. Appl. Phys. **136**, 105103 (2024); doi: 10.1063/5.0218950
Submitted: 14 May 2024 · Accepted: 23 August 2024 ·
Published Online: 9 September 2024

View Online Export Citation CrossMark

P. Dumas,[1,a)] F. Gustavo,[1] M. Opprecht,[1] G. Freychet,[1] P. Gergaud,[1] S. Kerdilès,[1] S. Guillemin,[1] J. L. Lábár,[2] B. Pécz,[2] F. Lefloch,[3] and F. Nemouchi[1]

AFFILIATIONS

[1]Université Grenoble Alpes, CEA LETI, 38000 Grenoble, France
[2]Institute for Technical Physics and Materials Science, HUN-REN Centre for Energy Research, 1121 Budapest, Hungary
[3]Université Grenoble Alpes, CEA IRIG, 38000 Grenoble, France

[a)]**Author to whom correspondence should be addressed:** paul.dumas2@cea.fr

ABSTRACT

Laser annealing was employed to trigger the solid-state reaction of a thin Co film (2.5 nm) with undoped Si. A metastable disilicide layer was obtained after one laser pulse close to the melt threshold. Its diffraction pattern, relaxed lattice parameter, and residual resisitivity are consistent with the formation of the defective CsCl structure. The $CoSi_2$ phase was found after prolonging the thermal treatment with additional pulses or rapid thermal annealing. Because CoSi is skipped in the phase sequence, $CoSi_2$ layers are more uniform in thickness, have an increased superconductivity and a reduced formation temperature. This approach is compatible with the SALICIDE process and can be used to form smooth contacts in superconducting or regular transistors.

© 2024 Author(s). All article content, except where otherwise noted, is licensed under a Creative Commons Attribution (CC BY) license (https://creativecommons.org/licenses/by/4.0/). https://doi.org/10.1063/5.0218950

10 September 2024 06:11:38

I. INTRODUCTION

For more than 50 years, transition metal silicides ($CoSi_2$, NiSi, PtSi, and $TiSi_2$) have been the materials of choice for contacting transistor terminals.[1,2] The Self-Aligned Silicide (SALICIDE) process is an essential part of the success of silicides. This straightforward process consists of making react a thin metal film with source, drain, and gate regions at elevated temperature. The self-aligned terminology is explained by the absence of photolithography step, the metal reacting with silicon but not with dielectrics. After thermal treatment, the unreacted metal is etched in a selective way so as to preserve the silicide lines. At the end of the 1990s, the Co SALICIDE process was the leading technology.[1,2] Cobalt monosilicide (CoSi) is formed after a first rapid thermal annealing (RTA) at around 500 °C. After selective etching, CoSi is transformed into cobalt disilicide (CoSi2) by a second RTA close to 700 °C.

Some limitations of the Co SALICIDE process originates from the formation of the monosilicide phase.[1,3] One of them is the presence of infrequent voids in narrow contact lines (<50 nm). These voids would originate from the agglomeration of vacancies generated during the formation of CoSi and/or from the lack of nucleation sites driving the CoSi to $CoSi_2$ transformation. This small concentration of nuclei is also responsible for the wavy interface that delimits $CoSi_2$ from Si. The wavy interfaces and especially the infrequent voids make the Co SALICIDE process unreliable on narrow contact dimensions. Ultimately, the compatibility of NiSi with SiGe substrates and the need for lower annealing temperatures precipitated the advent of the Ni SALICIDE process at the beginning of the 2000s.

The growing trend for superconducting technology is somehow renewing the interest in $CoSi_2$.[4,5] The aim of our team is to elaborate Silicon Josephson field effect transistors, which feature superconconducting source/drain such as V_3Si, PtSi, $CoSi_2$, and Si:B.[6–9] Among these, V_3Si has by far the highest critical temperature ($T_C \sim 17$ K), which is desirable for facilitating the transport of Cooper pairs as they get through the channel. Unfortunately, the realization of pure V_3Si contacts is made difficult by the rapid nucleation of VSi_2.[7] As for Si:B, the necessity of melting the source/drain regions while preserving the integrity of the gate is a tricky task. In contrast, the realization of PtSi or $CoSi_2$ contacts through the SALICIDE process is quite straightforward. In this work, we report the use of laser annealing to trigger the solid-state formation

© Author(s) 2024

of thin $CoSi_2$ films. The fact that CoSi is skipped in the phase sequence has positive consequences for Co silicidation.

II. MATERIALS AND METHODS

We started with two 300 mm Silicon On Insulator (SOI) wafers featuring a 33 nm thick (100) Si film on top of a 20 nm thick Buried Oxide Layer (BOX). The residual boron concentration in both SOI and substrate (775 μm) is close to 10^{15} cm^{-3} (<0.1 ppm). First, a cleaning sequence composed of HF and standard cleaning 1 was applied to remove the native oxide and regrow a thin suboxide at the SOI surface. The purpose of the suboxide is to reduce the rugosity of the resulting $CoSi_2$ layer.[1] Immediately after surface preparation, a thin Co film (2.5 nm) and a protective TiN layer (10 nm) were sputtered.

The thermal treatment of the conventional SALICIDE process was replicated on one wafer through a two-step RTA (480 and 700 °C for 10 s) in a N_2 atmosphere with a heating ramp of 20 °C/s. The second wafer was irradiated locally (15×15 mm^2fields) by a laser beam ($\lambda = 308$ nm) in a N_2 ambient. The full width at half maximum of the pulse is 160 ns, and the beam homogeneity is higher than 97.5%. One field may receive several pulses at a rate of 4 Hz and in a range of energy density between 400 and 900 mJ/cm^2. The beam switches from one field to another at a frequency of 1 Hz, and during each pulse, the reflectance is *in situ* monitored by time-resolved reflectometry (TRR) using a second laser ($\lambda = 635$ nm). Finally, the field irradiated with one pulse at 700 mJ/cm^2 was further treated by RTA (850 °C for 1 s) with the same heating ramp of 20 °C/s.

Samples were characterized by four-point probe measurements at room temperature (with TiN) and down to 350 mK (without TiN). TiN was etched in a room temperature solution of $NH_40H/H_20_2/H_20$ with volume ratios of 1:1:1 for 30 min. Scanning transmission electron microscopy (STEM) images were recorded using a high-angle annular dark-field detector and an acceleration energy of 200 keV. An energy-dispersive spectroscopy (EDS) analysis was performed along STEM characterization. X-ray diffraction (XRD) measurements were carried at Kα radiation ($\lambda = 1.5406$ Å) using two configurations: grazing incidence and in-plane. In the former, the angle between the incident beam and the sample surface is fixed at $\omega = 0.4°$. Both incident and diffracted beam are coplanar with the normal to the surface, and measured planes are tilted by $\theta - \omega$ relatively to the surface with θ being Bragg's angle. The in-plane configuration is non-coplanar, and both incident and diffracted beam are nearly parallel to the surface (few 0.1°). Here, measured planes are quasi-perpendicular to the surface.

Finally, we performed simulations through a Technology Computer Aided Design (TCAD) package[10] in order to assess the temperature inside the Co layer during the first laser pulse. The entire as-deposited stack (TiN/Co/SOI/BOX/substrate) was considered for simulating the temperature evolution. Because the metal layer is very thin, the temperature is nearly constant with a tiny gap of 1 °C between the surface and the bottom. Along the article, we will refer to simulated data presented in Fig. 1.

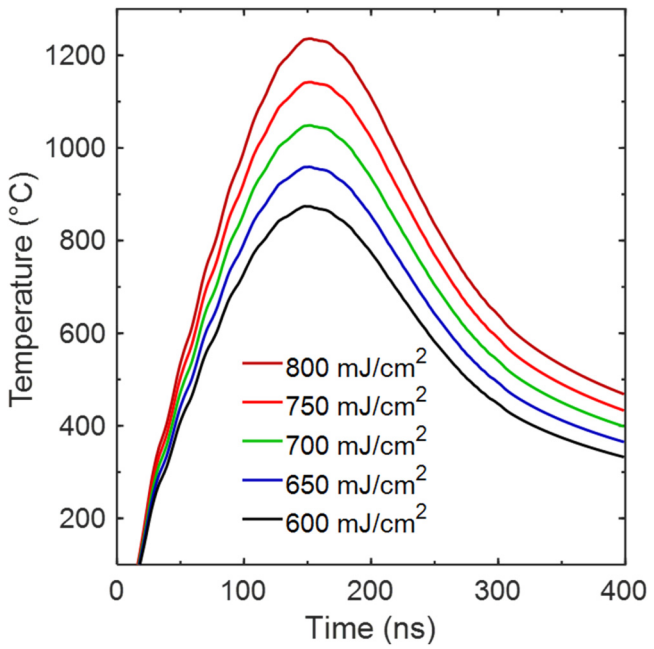

FIG. 1. Evolution of the mean temperature inside the 2.5 nm thick Co layer during the first laser pulse (TCAD simulations).

III. RESULTS AND DISCUSSION

A. Triggering silicidation below the melt threshold

In a first phase, we assessed the effect of the laser energy density (ED) on the reflectivity and room-temperature sheet resistance (R_S) of the TiN/Co/SOI stack. Results are shown in Figs. 2(a) and 2(b), respectively. In the range of 400–750 mJ/cm^2, the TRR signal slightly increases from 0.25 to 0.32 V before decreasing back to 0.25 V after 300 ns. This trend can be attributed to the heating/cooling cycle experienced by the stack in the solid state.[11,12] In parallel, the fact that R_S remains close to the as-deposited value (ED < 550 mJ/cm^2) before decreasing to a minimum of 48 Ω/sq (ED = 750 mJ/cm^2) is indicative of the formation of the lowly resistive $CoSi_2$ phase.

In the range of 775–900 mJ/cm^2, the TRR map features a high-intensity signal that indicates that the top layers went through the liquid state.[11,12] According to the work of Baeri,[13] the liquid phase propagates from the metal/Si interface at the temperature of the deepest eutectic point. For the Co–Si system, this eutectic corresponds to a Si content of 23 at. % and a temperature of 1205 °C.[14] This value is in good agreement with the peak temperature obtained by simulation at 800 mJ/cm^2 (Fig. 1). Moreover, this temperature being well below the melting point of TiN (~3000 °C), we expect no morphological degradation of the top layer. From Fig. 2(b), it is also apparent that the use of laser annealing above the melt threshold in the range of 775–900 mJ/cm^2 leads to a resistive stack ($R_S \sim 100$ Ω/sq).

10 September 2024 06:11:38

© Author(s) 2024

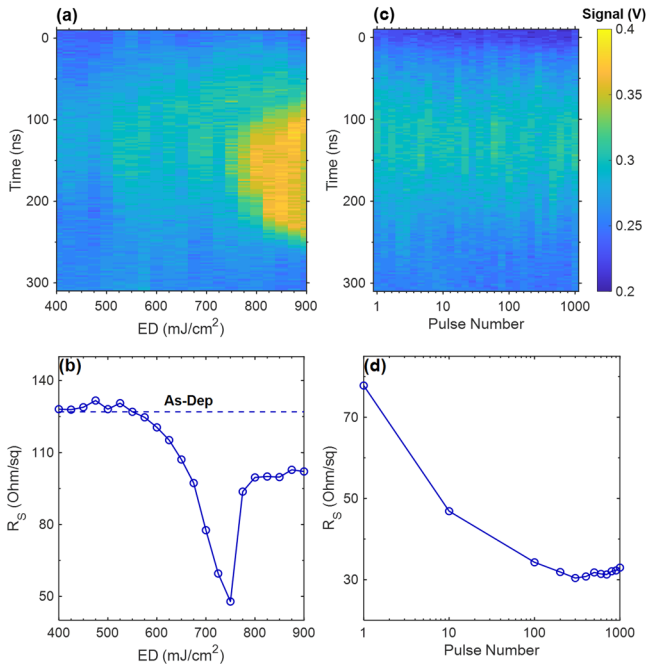

FIG. 2. TRR map and room temperature sheet resistance (TiN included) related to single-pulse experiments [(a) and (b)] and multi-pulse experiments [(c) and (d)]. In (c), the x-axis scale is linear between two successive powers of tens.

In a second phase, laser annealing was employed in multi-pulse mode in the aim of forming $CoSi_2$ in the solid state at different stages of growth. Fields were irradiated up to 1000 times at 700 mJ/cm^2. As confirmed by the absence of high-intensity TRR signal [Fig. 2(c)], the multi-pulse treatment did not trigger the melting of materials. R_S continuously decreases down to 30 Ω/sq with increasing the number of pulses up to 300, in agreement with the progressive formation of $CoSi_2$. Beyond 300 pulses, the near-constant R_S suggests that the formation of $CoSi_2$ is completed.

B. Morphology and natures of silicides

In what follows, S1, S10, and S100 refer to samples treated with 1, 10, and 100 pulses at 700 mJ/cm^2. The sample called SREF originates from the wafer treated with two-step RTA. Figure 3 regroups the cross section STEM images and EDS elemental profiles (at. %) related to SREF, S1 and S100. After two-step RTA, the STEM images reveal a dark thin layer (3.5 nm) below the TiN film. According to EDS, the composition of the latter is SiN with a small amount of O, Co, and Ti The relatively high O content (~10 at .%) most likely originates from the suboxide left by surface preparation. Also, please have in mind that the concentration ratio between Ti and N might proves to be erroneous due to the overlap between N Kα (0.392 keV) and Ti Lα (0.452 keV) radiations. Below the SiN film, one observes a bright layer with an averaged thickness of 9 nm. The EDS profile indicates a Si/Co ratio around two, hence corroborating the formation of $CoSi_2$. The wavy interface between $CoSi_2$ and Si is characteristic of the lack of nuclei driving the CoSi to $CoSi_2$ transformation.[1–3]

After one pulse, the composition of the sandwiched dark layer is unchanged (SiN), but its thickness is reduced (1.5 nm). This means that less Si was consumed during thermal treatment, in agreement with the deeper position of the SOI/BOX interface as shown by STEM. Furthermore, one unexpected commonality between S1 and SREF is the nature and thickness of the silicide layer. Indeed, it is puzzling to see that a single laser pulse is sufficient for completing the solid-state transformation of Co into a 9 nm thick $CoSi_2$ film. Besides, the interface between $CoSi_2$ and Si is rather sharp. The rapid decrease in Co concentration around 20 nm corroborates this point. This sharper interface is indicative of an increased proportion of $CoSi_2$ nucleation sites. This happens when the monosilicide phase (CoSi) is bypassed in the phase sequence or, in other words, when the disilicide phase ($CoSi_2$) is formed directly from the reaction of Co with Si.[15]

After 100 pulses, the SiN layer is a bit thicker (2 nm) because of the longer laser treatment. Furthermore, the slightly more wavy interface between $CoSi_2$ and Si could be a sign of the early stage of silicide agglomeration. One commonality between the three EDS profiles is the presence of a 5 nm Co tail (<10 at. %) at the $CoSi_2$/Si interface. We attribute this tail to the coexistence of Si and $CoSi_2$ in the direction normal to the TEM lamella. Such $CoSi_2$ overgrowth might originate from inhomogeneities in deposited Co thickness. This issue arises from our sputtering machine that is not designed for depositing such a small metal thickness. Finally, it is difficult to understand why S100 is much less resistive than S1 [Fig. 1(d)] since the stack of materials appears to be the same (10 nm TiN/9 nm $CoSi_2$/SOI). In order to resolve this point, samples were further characterized by XRD.

At the time of the XRD analysis, S10 and S100 were TiN-free because of an early low-temperature characterization. Figure 4(a) shows the XRD patterns obtained in the grazing incidence configuration. Peaks located at 36.5° and 42.5° correspond to TiN (111) and (200) reflections. Black arrows indicate the three main reflections of the fluorite structure in which $CoSi_2$ crystallizes at equilibrium. While the (220) peak is well marked on all spectra, the (111) reflection is nearly absent in the S1 pattern and is weak in the S10 pattern. The same trend is observed for the (311) reflection even though the peaks are much less intense. The lower intensity of *odd* (hkl) reflections observed in S1 and S10 patterns is characteristic of the defective CsCl structure, a crystal lattice in which $CoSi_2$ crystallizes in non-equilibrium conditions.[16] Another metastable structure in which $CoSi_2$ might crystallize is the so-called "adamentane" in which Co atoms occupy the tetrahedral interstitial sites of the Si diamond lattice.[17] By evaluating the structure factor of this structure, one finds that the intensities of (200) and (220) peaks are of the same order of magnitude. Since there is no (200) peak in Fig. 4(a), we conclude that the silicides did not crystallize in the adamentane structure.

In what follows, the notation $Co_{0.5}Si$ will be used to refer to the defective CsCl structure. In this crystal, there is twice as more Si as Co because half of cation sites is vacant. The "defective" terminology accounts for this very large concentration of Co vacancies

10 September 2024 06:11:38

© Author(s) 2024

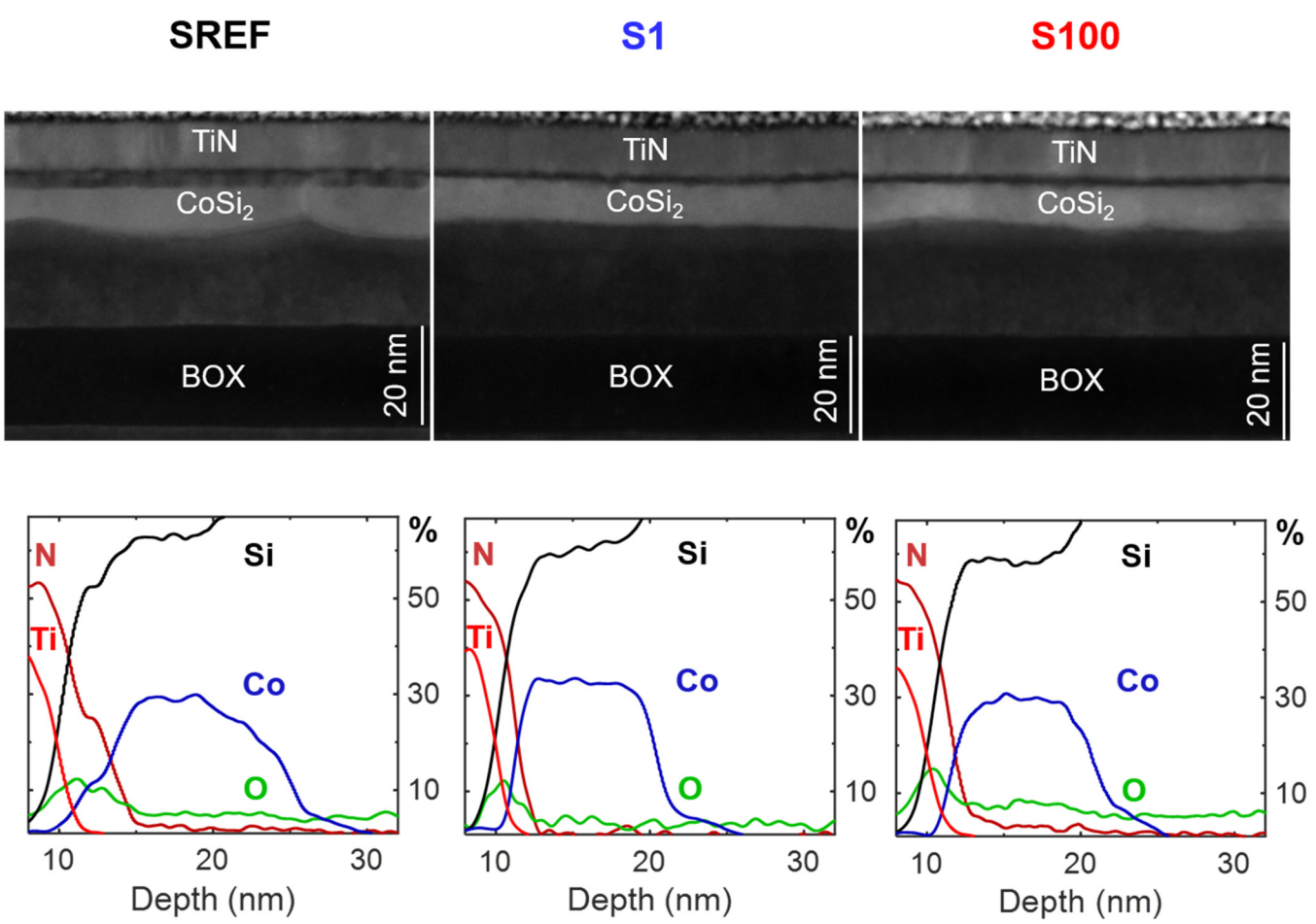

FIG. 3. Cross-sectional STEM image and EDS profiles related to SREF, S1 and S100. The depth origin in EDS profiles is situated at the TiN surface.

and for the high resistivity of this phase. In addition, one has to keep in mind that the defective CsCl structure is highly disordered due to the random distribution of Co atoms. To support the thesis of $Co_{0.5}Si$ formation, one can derive the lattice parameter (a_0) of the relaxed disilicide film,

$$a_0 = \frac{1-\nu}{1+\nu} a_\perp + \frac{2\nu}{1+\nu} a_{//}\,, \tag{1}$$

where $\nu = 0.33$ is the reported Poisson's ratio for $Co_{0.5}Si$ and $CoSi_2$ and[16,18] $a_\perp$ and $a_{//}$ are the out-of-plane and in-plane lattice parameter, respectively. First, a lattice parameter a_G was computed from the grazing incidence configuration. The (220) peak that is common to all samples was fitted with a sum of Gaussian and Loretzian function,[19] and the $2\theta_G$ corresponding to the maximum intensity was extracted [Fig. 4(b)]. We followed the same procedure for extracting $a_{//}$ from the in-plane configuration [Fig. 4(c)]. Finally, we used the $\sin^2\psi$ relation for deriving $a_\perp$,[20]

$$a_\perp = \frac{a_G - a_{//}\sin^2\psi}{\cos^2\psi}\,, \tag{2}$$

where $\psi = \theta_G - \omega$ is the tilt angle of diffracting (220) planes.

Results are shown in Table I. After a two-step RTA, a_0 is close to the reported value of the fluorite structure (5.364 Å),[21] hence corroborating the formation of $CoSi_2$. After one laser pulse, however, a_0 is slightly higher and matches well with the lattice parameter of $Co_{0.5}Si$ (5.38 Å).[16] After 10 and 100 pulses, a_0 progressively decreases down to the fluorite value, hence indicating the transformation of $Co_{0.5}Si$ into $CoSi_2$. The increase in *odd* (hkl) reflections [Fig. 4(a)] and decrease in R_S [Fig. 1(d)] support this result.

Following the results of Goncalves-Conto *et al.*,[16] we tested a more standard annealing method for transforming $Co_{0.5}Si$ into $CoSi_2$. In this respect, a sample called S1+ was obtained by further

10 September 2024 06:11:38

© Author(s) 2024

annealing S1 with RTA (850 °C for 1 s). From XRD, we identified the fluorite structure with $a_{//} = 5.387$ Å ($2\theta_{//} = 47.71 \pm 0.01°$), relatively close to the relaxed lattice parameter of $CoSi_2$ ($a_0 = 5.364$ Å). In Sec. III C, it will be shown that this small gap between $a_{//}$ and a_0 plays a decisive role in enhancing the superconductivity of $CoSi_2$.

C. Properties of disilicide films

Properties of disilicides were assessed using various characterizations. The lateral crystallite size (CS) was evaluated from the in-plane (220) peak using the Scherrer equation.[22] As seen in

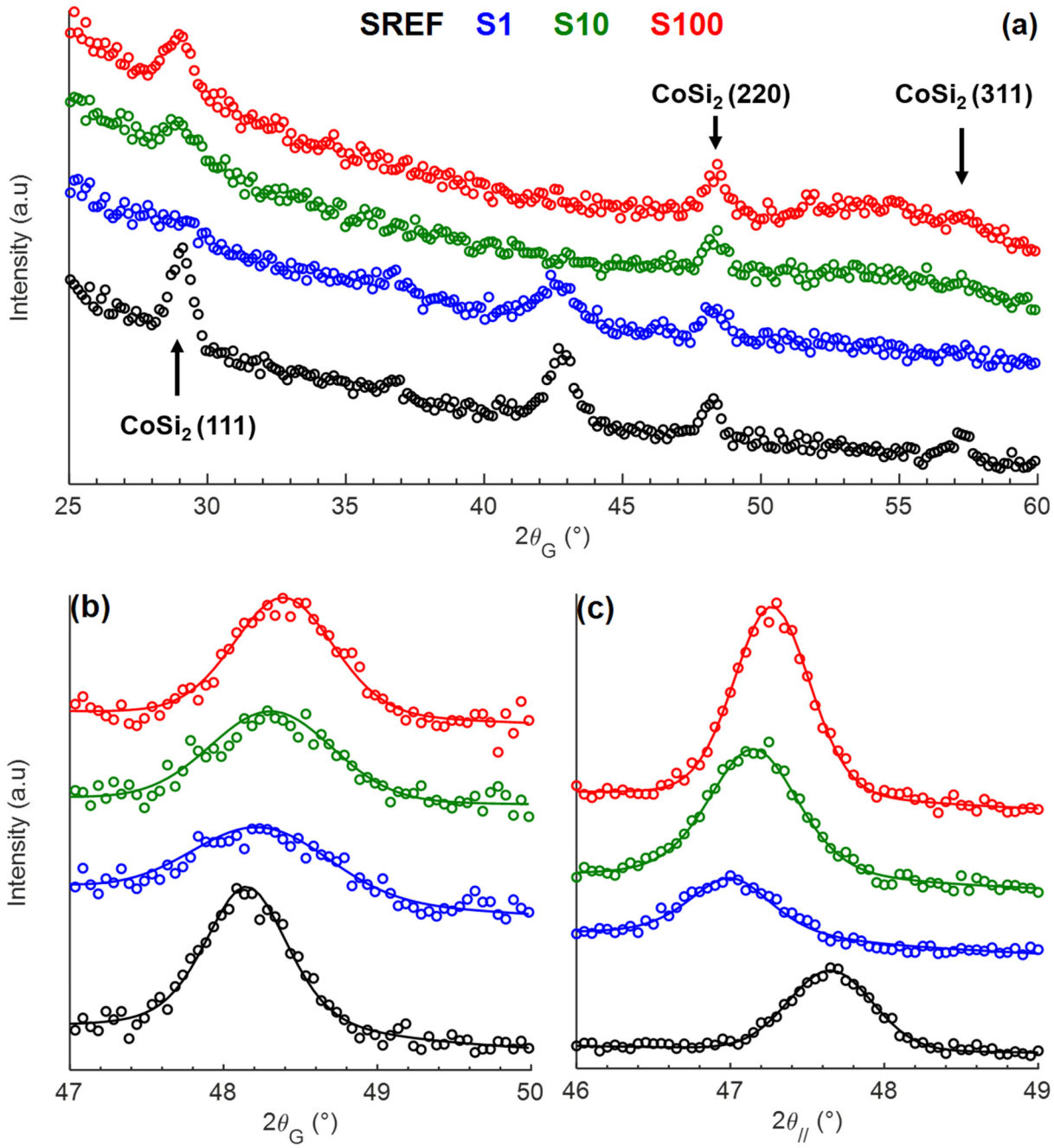

FIG. 4. (a) Grazing incidence XRD patterns related to SREF, S1, S10, and S100. (b) Focus on grazing incidence (220) peaks. (c) Focus on in-plane (220) peaks.

10 September 2024 06:11:38

© Author(s) 2024

TABLE I. Values extracted from XRD.

	$2\theta_G$ (±0.01°)	$2\theta_{//}$(± 0.01°)	a_0 (±0.02 Å)
SREF	48.15	47.65	5.362
S1	48.24	47	5.384
S10	48.31	47.15	5.373
S100	48.39	47.27	5.363

Table II, CS is almost invariant to annealing conditions (~14 nm). Therefore, we exclude this parameter from being responsible for the variations in electrical properties as shown later on. Then, we evaluated the residual in-plane strain $\varepsilon_{//} = (a_{//} - a_0)/a_0$. As seen in Table II, $\varepsilon_{//}$ is two to three times higher in films treated with laser annealing. To understand why, let us recall that $\varepsilon_{//}$ is the sum of an intrinsic and thermal contribution.[24–26] The intrinsic strain arises from the volume variation experienced by Co upon transforming into a silicide. In general, this contribution fully relaxes close to the formation temperature (T_F) of the silicide.[24] When the temperature drops from T_F to 20 °C, a thermal strain builds up,

$$\varepsilon_T\,(\mathrm{RTA}) = (\alpha_F - \alpha_S) \times (T_F - 20\ ^\circ\mathrm{C}), \tag{3.1}$$

$$\varepsilon_T\,(\mathrm{LA}) = \alpha_F \times (T_F - 20\ ^\circ\mathrm{C}), \tag{3.2}$$

where α_F and α_S are the expansion coefficient of $CoSi_2$[27] and Si,[28] respectively. In the case of S1, S10, and S100, the strain is higher because the substrate is unheated during laser annealing [Eq. (3.2)]. Let us now evaluate ε_T from these equations. According to Fig. 1, the peak temperature experienced by Co upon the first laser pulse at 700 mJ/cm^2 is close to 1050 °C. The heating ramp being extremely fast (~10^{10} K/s), we assume that the $Co_{0.5}Si$ film formed at this temperature. As for SREF, $CoSi_2$ is expected to form from CoSi at around 600 °C[1] during the heating ramp of the second RTA. The calculation yields ε_T (S1) = 1.48% and ε_T (SREF) = 0.62%, in close agreement with experimental strains (Table II). We conclude that the strain is essentially thermal in S1 and SREF.

Assuming a full contribution of thermal strain in all disilicides, one can estimate T_F using Eqs. (3.1) and (3.2). Results are shown in Table II. Perhaps the most important result is the smaller T_F of $CoSi_2$ when the starting phase is $Co_{0.5}Si$ (~450 °C for S1+) in place of CoSi (~550 °C for SREF). First, this result suggests that the temperature employed for forming S1+ (850 °C) is unnecessarily high. Second, this means that the second annealing of Co silicidation can be performed at a smaller temperature, provided that the $Co_{0.5}Si$ phase is formed upon first annealing.

After TiN etching, the resistivity (ρ) of disilicides was measured down to 350 mK. The evolution of ρ between 0.5 and 1.5 K is shown in Fig. 5. After one pulse, ρ is constant and corresponds to the so-called residual resistivity (ρ_0). Again, this high ρ_0 (123 μΩ cm) is consistent with the formation of $Co_{0.5}Si$.[16] After 10 and 100 pulses, ρ_0 is scaled by two and four, respectively. Despite this marked decrease in ρ_0, the residual-resistance ratio (RRR) increases slightly from 1.1 to 1.4. This suggests that the crystalline quality of the film did not significantly improve with multi-pulse processing, despite the disappearance of vacancies through the transformation of $Co_{0.5}Si$ into $CoSi_2$. Our interpretation is that the laser treatment injects additional defects such as quenched-in vacancies.[29,30]

As shown in Fig. 5 and Table II, further annealing S1 with RTA leads to a small ρ_0 (13.5 μΩ cm) and to a doubling of RRR. This time, the crystal has been well repaired. Yet, the film is a bit more resistive and of lower quality in comparison to SREF. One can argue that the hot RTA (850 °C) is at the origin of these poorer properties through the morphological degradation of the film. Still, $CoSi_2$ layers are known to resist temperatures up to 950 °C when capped by a 10 nm thick TiN layer,[31] making agglomeration unlikely in our case. Another explanation might arise from the persistence of $Co_{0.5}Si$ regions. This issue has been reported after annealing thin $Co_{0.5}Si$ films at 650 °C for 30 min.[16] Perhaps our RTA treatment was not sufficient for completely transforming the $Co_{0.5}Si$ phase.

If we now compare our best RRR value with those already published, one sees a close agreement with the recent work of Chiu *et al.*[4] who employed a cleaner annealing atmosphere for forming 9.5 nm thick $CoSi_2$ layers. As for the 10 nm thick epitaxial $CoSi_2$ layers obtained by Badoz *et al.*,[23] the RRR is high (~4) and the ρ_0 is low (4 μΩ cm) because of the films' extreme cleanliness and almost perfect crystalline quality. Nevertheless, this sophisticated process is far from being compatible with the constraints of the microelectronics industry.

Finally, we can assess the superconductivity of disilicides from the resistivity curves shown in Fig. 5. Following the standard convention, one defines the critical temperature (T_C) as the temperature at which ρ_0 drops by a half. S1 does not show sign of superconductivity down to 380 mK. We attribute this result to the

TABLE II. Properties of thin disilicide films (~9 nm). NS stands for non-superconducting.

Samples	CS (nm)	$\varepsilon_{//}$ (%)	T_F (°C)	ρ_0 (μΩ cm)	RRR	T_C (K)
S1	14	1.49	1050	123	1.1	NS
S10	13	1.38	980	53	1.3	NS
S100	15	1.31	930	28	1.4	0.65
SREF	13.5	0.56	540	8	2.9	1.05
S1+	14	0.43	420	13.5	2.2	1.30
Ref. 23	/	~1.20 (Epitaxial)	/	4	4	0.85
Ref. 4	/	/	~550	13.5	3	1.25

10 September 2024 06:11:38

© Author(s) 2024

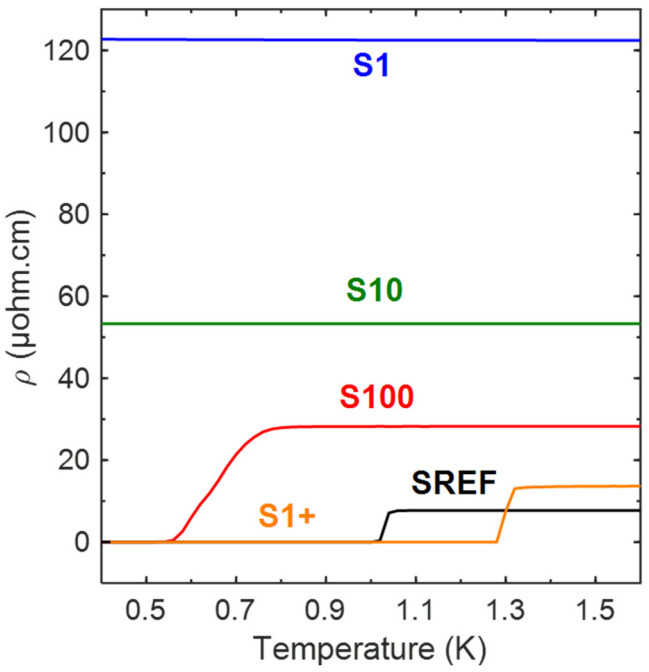

FIG. 5. Evolution of the disilicide resistivity between 0.5 and 1.5 K.

resistive behavior of the defective CsCl structure. The same trend is evidenced for S10. Here, we believe that the volume fraction of $CoSi_2$ is too small to form a continuous superconducting path. After 100 pulses, a broad superconducting transition is observed at $T_C = 0.65$ K. In our understanding, this broadening is characteristic of an inhomogeneous film featuring various degrees of superconductivity. Laser-induced defects could be at the origin of this phenomenon.

As for SREF and S1+, a sharper superconducting transition is observed at $T_C = 1.05$ and 1.3 K, respectively. By comparing the values listed in Table II, one arrives at the rather surprising conclusion that the T_C does not follow ρ_0 nor RRR trend. In other words, the quality of the film is no guarantee of a high T_C. Instead, there is a clear correlation between superconductivity and strain, such as the lower the strain, the higher the T_C. Even though no strain was reported by Chiu *et al.*,[4] the same group claims elsewhere that they succeeded in reducing the strain by increasing the annealing duration.[32] Finally, it is worth mentioning that this correlation between strain and superconductivity has been demonstrated in other materials such as V_3Si,[33] FeSe,[34] and $SrTiO_3$.[35]

IV. CONCLUSION

In summary, we have developed an alternative thermal treatment for Co silicidation. After one laser pulse (160 ns) below the melt threshold of materials, a metastable disilicide layer was obtained. Atoms reorganize into the stable fluorite structure ($CoSi_2$) by prolonging the thermal treatment with additional pulses or RTA. In the former case, the resulting layers are of poor crystalline quality (RRR ~ 1), probably because of laser-induced defects. In the latter case, the quality is much improved (RRR ~ 2) even though some metastable regions are thought to remain.

The fact that CoSi is skipped in the phase sequence has positive consequences for Co silicidation. First, $CoSi_2$ films are more uniform in thickness, and the voiding issue encountered in small contact dimensions should be alleviated if not solved. Second, the formation temperature of $CoSi_2$ is reduced (~100 °C smaller), which is advantageous for lowering the thermal budget of Co silicidation. Third, the superconducting critical temperature of $CoSi_2$ is enhanced through a reduction in thermal strain.

ACKNOWLEDGMENTS

The authors would like to thank SCREEN company and its French subsidiary LASSE for helping in operating and maintaining the LT-3100 laser annealing system. This work was founded by European projects MATQu and SIQUOS (Grant Agreement Nos. 101007322 and 101017733).

AUTHOR DECLARATIONS

Conflict of Interest

The authors have no conflicts to disclose.

Author Contributions

P. Dumas: Formal analysis (lead); Investigation (lead); Writing – original draft (lead). **F. Gustavo:** Data curation (lead). **M. Opprecht:** Data curation (lead); Formal analysis (supporting). **G. Freychet:** Data curation (equal); Formal analysis (equal). **P. Gergaud:** Data curation (supporting); Formal analysis (lead); Writing – original draft (supporting). **S. Kerdilès:** Formal analysis (supporting); Resources (lead). **S. Guillemin:** Data curation (equal). **J. L. Lábár:** Data curation (lead); Formal analysis (supporting). **B. Pécz** Data curation (supporting); Formal analysis (supporting). **F. Lefloch:** Project administration (lead); Supervision (lead). **F. Nemouchi:** Project administration (lead); Supervision (lead); Writing – original draft (supporting).

DATA AVAILABILITY

The data that support the findings of this study are available within the article and from the corresponding author upon reasonable request.

REFERENCES

[1]C. Lavoie, F. M. d'Heurle, and S. L. Zhang, "Silicides," in *Handbook of Semiconductor Manufacturing Technology* (CRC Press, 2017), pp. 10–11.
[2]S. L. Zhang and M. Östling, "Metal silicides in CMOS technology: Past, present, and future trends," Crit. Rev. Solid State Mater. Sci. **28**(1), 1–129 (2003).
[3]C. Lavoie, F. M. d'Heurle, C. Detavernier, and C. Cabral, Jr., "Towards implementation of a nickel silicide process for CMOS technologies," Microelectron. Eng. **70**(2–4), 144–157 (2003).
[4]S. P. Chiu, C. J. Wang, Y. C. Lin, S. T. Tu, S. K. Sahu, R. T. Wang, C.-Y. Wu, C.-Y. Yeh, S. Kirchner, and J. J. Lin, "Electronic and superconducting properties of $CoSi_2$ films on silicon—An unconventional superconductor with technological potential," Chin. J. Phys. **90**, 348–363 (2024).

10 September 2024 06:11:38

© Author(s) 2024

[5]E. Mukhanova, W. Zeng, E. A. Heredia, C. W. Wu, I. Lilja, J. J. Lin, S. S. Yeh, and P. Hakonen, "Kinetic inductance in superconducting $CoSi_2$ coplanar microwave transmission lines," APL Mater. **12**, 4 (2024).
[6]Y. Yao, D. F. Fernandes, T. Košutová, T. Kubart, Z. Zhang, F. Lefloch, and S. L. Zhang, "Self-aligned formation of superconducting sub-5 nm PtSi films," APL Quantum **1**, 2 (2024).
[7]T. D. Vethaak, F. Gustavo, T. Farjot, T. Kubart, P. Gergaud, S. L. Zhang, F. Lefloch, and F. Nemouchi, "Superconducting V_3Si for quantum circuit applications," Microelectron. Eng. **244**, 111570 (2021).
[8]F. Chiodi, J. E. Duvauchelle, C. Marcenat, D. Débarre, and F. Lefloch, "Proximity-induced superconductivity in all-silicon superconductor/normal-metal junctions," Phys. Rev. B **96**(2), 024503 (2017).
[9]P. Dumas, M. Opprecht, S. Kerdilès, J. Lábár, B. Pécz, F. Lefloch, and F. Nemouchi, "Superconductivity in laser-annealed monocrystalline silicon films: The role of boron implant," Appl. Phys. Lett. **123**, 13 (2023).
[10]K. Huet, J. Aubin, P. E. Raynal, B. Curvers, A. Verstraete, B. Lespinasse, F. Mazzamuto, A. Sciuto, S. F. Lombardo, A. La Magna, P. Acosta-Alba, L. Dagault, C. Licitra, J.-M. Hartmann, and S. Kerdilès, "Pulsed laser annealing for advanced technology nodes: Modeling and calibration," Appl. Surf. Sci. **505**, 144470 (2020).
[11]P. Acosta Alba, J. Aubin, S. Perrot, F. Mazzamuto, A. Grenier, and S. Kerdilès, "Solid phase recrystallization induced by multi-pulse nanosecond laser annealing," Appl. Surf. Sci. Adv. **3**, 100053 (2021).
[12]L. Casiez, N. Bernier, J. Chrétien, J. Richy, D. Rouchon, M. Bertrand, F. Mazen, M. Frauenrath, A. Chelnokov, J. M. Hartmann, V. Calvo, N. Pauc, V. Reboud, and P. Acosta Alba, "Recrystallization of thick implanted GeSn layers with nanosecond laser annealing," J. Appl. Phys. **131**, 15 (2022).
[13]P. Baeri, "Pulsed laser induced modifications of metal silicide layers," Thin Solid Films **241**(1–2), 142–150 (1994).
[14]K. Ishida, T. Nishizawa, and M. E. Schlesinger, "The Co-Si (Co-silicon) system," J. Phase Equilib. **12**, 578–586 (1991).
[15]A. Vantomme, S. Degroote, J. Dekoster, G. Langouche, and R. Pretorius, "Concentration-controlled phase selection of silicide formation during reactive deposition," Appl. Phys. Lett. **74**(21), 3137–3139 (1999).
[16]S. Goncalves-Conto, U. Schärer, E. Müller, H. von Känel, L. Miglio, and F. Tavazza, "Competitive metastable phase in low-temperature epitaxy of $CoSi_2$/Si (111)," Phys. Rev. B **55**(11), 7213 (1997).
[17]S. L. Zhang, J. Cardenas, F. M. d'Heurle, B. G. Svensson, and C. S. Petersson, "On the formation of epitaxial $CoSi_2$ from the reaction of Si with a Co/Ti bilayer," Appl. Phys. Lett. **66**(1), 58–60 (1995).
[18]G. Guénin, M. Ignat, and O. Thomas, "Determination of the elastic constants of a Co disilicide intermetallic compound," J. Appl. Phys. **68**(12), 6515–6516 (1990).
[19]M. Hecq, "A fitting method for X-ray diffraction profiles," J. Appl. Crystallogr. **14**(1), 60–61 (1981).
[20]I. C. Noyan and J. B. Cohen, *Residual Stress: Measurement by Diffraction and Interpretation* (Springer, 2013).
[21]W. Wong-Ng, H. F. McMurdie, B. Paretzkin, C. R. Hubbard, A. L. Dragoo, and J. M. Stewart, "Standard X-ray diffraction powder patterns of fifteen ceramic phases," Powder Diffr. **2**(2), 106–117 (1987).
[22]A. L. Patterson, "The Scherrer formula for X-ray particle size determination," Phys. Rev. **56**(10), 978 (1939).
[23]P. A. Badoz, A. Briggs, E. Rosencher, and F. Arnaud d'Avitaya, "Superconductivity in ultra-thin $CoSi_2$ epitaxial films," J. Phys. Lett. **46**(20), 979–983 (1985).
[24]A. Steegen and K. Maex, "Silicide-induced stress in Si: Origin and consequences for MOS technologies," Mater. Sci. Eng., R **38**(1), 1–53 (2002).
[25]F. M. D'Heurle and O. Thomas, "Stresses during silicide formation: A review," in *Defect and Diffusion Forum* (Trans Tech Publications Ltd, 1996), Vol. 129, pp. 137–150.
[26]O. Thomas, P. Gergaud, C. Rivero, and F. M. d'Heurle, "Stress development during the reactive formation of silicide films," in *Defect and Diffusion Forum* (Trans Tech Publications Ltd, 2005), Vol. 237, pp. 801–812.
[27]D. Smeets, G. Vanhoyland, J. D'Haen, and A. Vantomme, "On the thermal expansion coefficient of $CoSi_2$ and $NiSi_2$," J. Phys. D: Appl. Phys. **42**(23), 235402 (2009).
[28]H. Watanabe, N. Yamada, and M. Okaji, "Linear thermal expansion coefficient of silicon from 293 to 1000 K," Int. J. Thermophys. **25**(1), 221–236 (2004).
[29]J. Takamura, "Quenched-in vacancies and quenching strains in gold," Acta Metall. **9**(6), 547–557 (1961).
[30]W. Hertz and H. Peisl, "Volume and electrical resistivity change due to vacancies in platinum," J. Phys. F: Met. Phys. **5**(4), 604 (1975).
[31]C. Detavernier, G. P. Ru, R. L. Van Meirhaeghe, and K. Maex, "The influence of Ti and TiN on the thermal stability of $CoSi_2$," MRS Online Proc. Libr. **670**, 1–6 (2001).
[32]C. J. Chiou, S. P. Chiu, J. J. Lin, and Y. C. Chou, "Effects of atomic scale imperfection at the interfaces of $CoSi_2$ and Si (100) on Schottky barrier contacts," CrystEngComm **17**(23), 4276–4280 (2015).
[33]T. D. Vethaak, F. Gustavo, T. Farjot, T. Kubart, P. Gergaud, S. L. Zhang, F. Nemouchi, and F. Lefloch, "Influence of substrate-induced thermal stress on the superconducting properties of V_3Si thin films," J. Appl. Phys. **129**, 10 (2021).
[34]Y. F. Nie, E. Brahimi, J. I. Budnick, W. A. Hines, M. Jain, and B. O. Wells, "Suppression of superconductivity in FeSe films under tensile strain," Appl. Phys. Lett. **94**, 24 (2009).
[35]K. Ahadi, L. Galletti, Y. Li, S. Salmani-Rezaie, W. Wu, and S. Stemmer, "Enhancing superconductivity in $SrTiO_3$ films with strain," Sci. Adv. **5**(4), eaaw0120 (2019).

10 September 2024 06:11:38

© Author(s) 2024